Photoabsorption by Neutral Argon Calculated by Many-Body Perturbation Theory*

Hugh P. Kelly and Raymond L. Simons
Department of Physics, University of Virginia, Charlottesville, Virginia 22901
(Received 18 December 1972)

The photoionization cross section for Ar I is calculated from threshold to 50 eV by means of many-body perturbation theory. Good agreement is obtained with the experimental data of Madden, Ederer, and Codling, including resonances. It is found that a low-order calculation is adequate.

Photoionization cross sections $\sigma(\omega)$ of atoms and molecules are of great use in many areas of physics.[1] They also are of considerable interest to both atomic experimentalists and theorists as a rich source of information on detailed atomic structure and processes. In the case of the rare gases there exist accurate experimental data[2-5] which present a strong challenge to atomic theorists.

Calculations on the neutral argon atom have been carried out in recent years by many authors.[6-12] Only those of Hartree-Fock (HF) accuracy[8,9,12] or greater[10,11] yielded qualitative agreement with experiment near threshold. The HF calculations have a discrepancy by approximately a factor of 2 between cross sections determined by "length" and "velocity" matrix elements.[13] Calculations by Amus'ya, Cherepkov, and Chernysheva[10] used the random-phase approximation with exchange (RPAE) and discretized the continuum. They proved that use of the RPAE gives identical results for length and velocity matrix elements. Their cross section from threshold to 40 eV is in very good agreement with experiment.[2,3]

Wendin[14] has calculated $\sigma(\omega)$ for Xe and concluded that one must include terms to infinite order in the Coulomb interaction in order to obtain accurate results. In the RPAE one is also summing certain classes of terms to all orders in the Coulomb interaction.

In the present work we investigate use of the many-body perturbation theory (MBPT) of Brueckner[15] and Goldstone[16] to calculate $\sigma(\omega)$ for Ar I. The MBPT is a Rayleigh-Schrödinger-type perturbation theory which has been adapted to the many-body problem by removal of the "unlinked clusters."[15,16] The unperturbed state is a determinant of single-particle states. Terms in the expansion are evaluated with single-particle states and are represented by diagrams. A detailed description of MBPT is given by Brueckner,[15] and applications to atoms are reviewed by Kelly.[17] We have previously used MBPT to calculate $\sigma(\omega)$ for Fe I[18] and O^-.[19] For $\sigma(\omega)$ one needs dipole (length) matrix elements $\langle\psi_k|\sum z_i|\psi_0\rangle$, where ψ_0 and ψ_k are initial and final (continuum) many-particle states. Dipole velocity matrix elements are obtained[13] by replacing z by $(d/dz)/i(E_k - E_0)$. We calculate $\langle\psi_k|\sum z_i|\psi_0\rangle$ by perturbation theory,[18] and in Fig. 1 we present many of the low-order diagrams for this expansion. There are also exchange diagrams corresponding to direct diagrams of Figs. 1(b)–1(f). The lowest-order diagram is shown in Fig. 1(a) and equals $\langle k|z|p\rangle$. In the remaining diagrams energy denominators are treated according to $(D+i\epsilon)^{-1} = PD^{-1} - i\pi\,\delta(D)$. Diagrams of first order in the Coulomb interaction are shown in Figs. 1(b) and

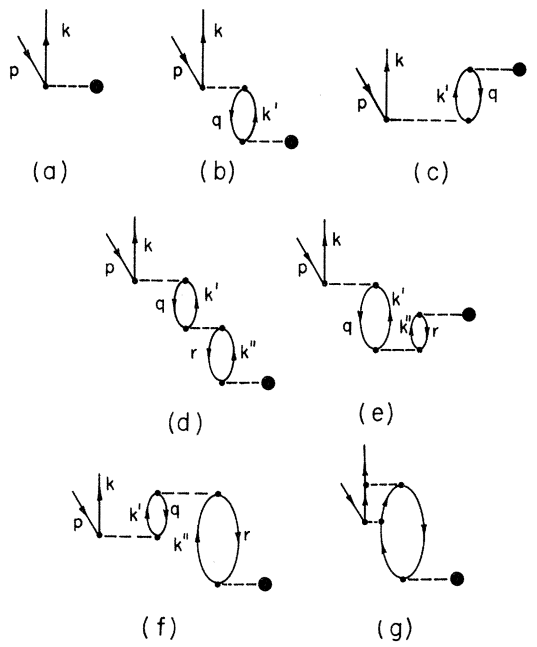

FIG. 1. Diagrams contributing to the matrix element $\langle\psi_k|\Sigma z_i|\psi_0\rangle$. Solid dot indicates matrix element of z. Other dashed lines represent Coulomb interactions. Exchange diagrams are also included.

1(c). Typical diagrams in the next order are shown in Figs. 1(d)–1(g). Diagrams (d)–(f) are included in the RPAE. Diagrams like Figs. 1(g) are not included by the RPAE and also were not included in this calculation. In addition to Fig. 1, we also include the normalization diagrams.[17]

We use our methods[17] for evaluating diagrams and calculate a "complete" set of radial functions for each l. Near threshold, $\sigma(\omega)$ is dominated by $3p \rightarrow kd$ transitions. The appropriate potential for kd states is the HF V^{N-1} potential[17] $V_{\mathrm{HF}}(l=2)$ arising from the $(3p)^5\,{}^2P kd\,{}^1P$ state. As pointed out by Amus'ya, Cherepkov, and Chernysheva,[10] $-\langle k|V_{\mathrm{HF}}(l=2)|k'\rangle$ cancels all corresponding matrix elements with passive unexcited states *and also* all Coulomb matrix elements of Fig. 1(b) when p and q both refer to $3p$ single-particle states with different m_l, m_s. This type of potential has also been proposed recently by Ishihara and Poe.[20]

In Fig. 2 the curves labeled HFL and HFV refer to $\sigma(\omega)$ obtained with diagram 1(d) with length and velocity matrix elements, respectively, and use of $V_{\mathrm{HF}}(l=2)$ for kd states. All curves also include $3p \rightarrow ks$ cross sections which contribute only 10% of $\sigma(\omega)$. The $3s \rightarrow kp$ cross section is included and contributes very little beginning with a threshold at 29.24 eV. Including diagrams 1(a) and 1(b), length and velocity curves agree to nearly 5% and also agree well with the experimental results shown in Fig. 2.

Our final correlated curves shown in Fig. 2 include all diagrams of the types shown in Figs. 1(a)–1(f) with $3s$ and $3p$ hole states. Exchange diagrams are also included. Because of our choice of potential, diagrams (b), (d), and (e) vanish when the hole states all refer to the same subshell. Normalization diagrams were included and reduce $\sigma(\omega)$ by 2.3%. With the exception of the resonances, the cross section is mostly affected by diagrams (a) and (c), thus indicating the importance of including ground-state corre-

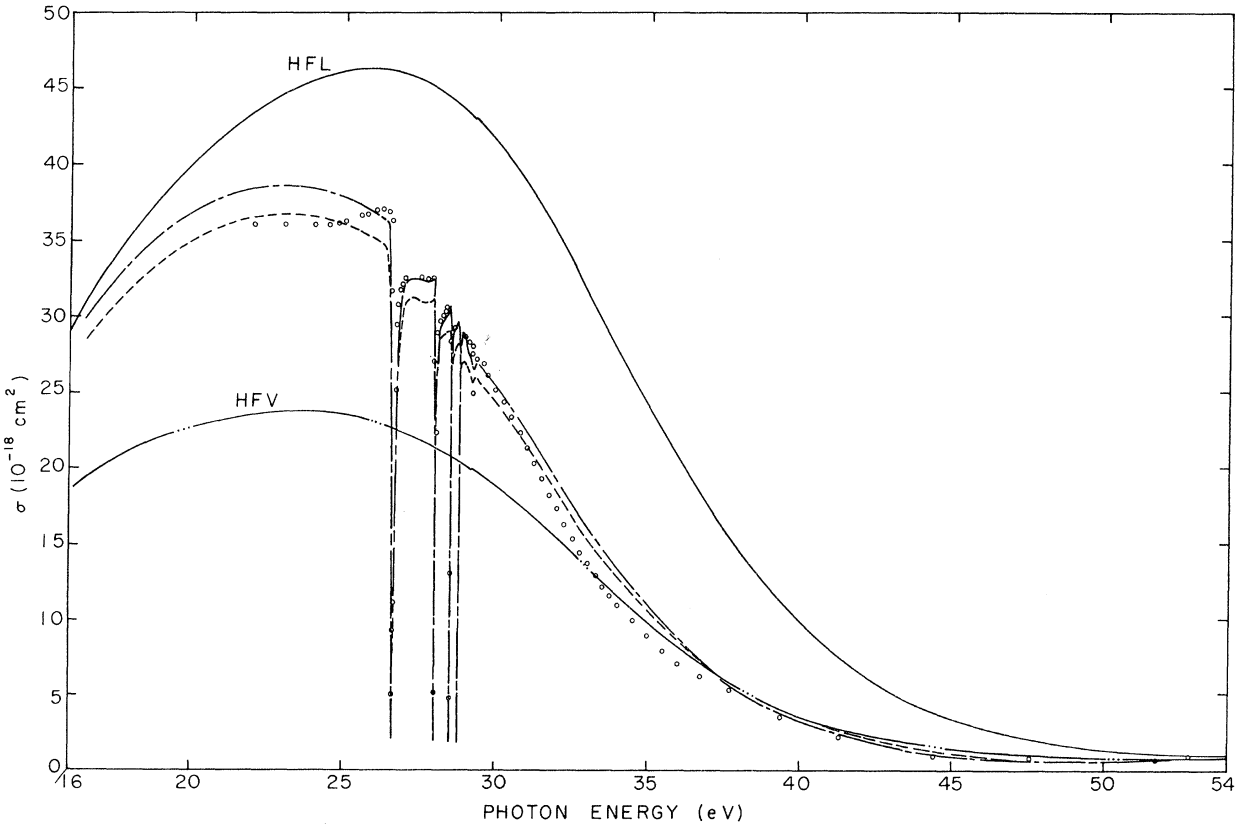

FIG. 2. Cross section σ for photoabsorption by ArI. HFL represents Hartree-Fock length cross section. HFV represents Hartree-Fock velocity cross section. Dot-dashed line, calculated length cross section including higher-order terms. Dashed line, calculated velocity cross section including higher-order terms. The circles represent experimental data from Ref. 3 (below 37 eV) and from Ref. 2 (above 37 eV). We have only shown the lowest $3s \rightarrow np$ resonances, there being an infinite number of them preceding the $3s$ threshold at 29.24 eV.

TABLE I. Resonance energies and widths for the $3s3p^6np^1P$ series in Ar I. All results are in electron volts.

State	E(calc)[a]	E(exp)[b]	Γ_n(calc)[c]	Γ_n(exp)[b]
$4p$	26.709	26.614	0.085 77	0.080 ± 0.005
$5p$	28.024	27.996	0.025 23	0.0282 ± 0.0013
$6p$	28.522	28.509	0.010 87	0.0126 ± 0.0012
$7p$	28.766		0.005 66	
$8p$	28.904		0.003 33	

[a]Resonance energy calculated semiempirically as described in text.
[b]Experimental results from Ref. 3.
[c]Resonance width.

lations. Diagram (f) improves agreement with experiment only in the range 30–45 eV.

Diagram (b) with $p = 3p$, $q = 3s$, and $k' = np$ is the lowest-order diagram contributing to the $3s3p^6np^1P$ resonances. Its energy denominator is $\epsilon_{3s} - \epsilon_{np} + \omega$. Including higher-order diagrams results[19] in a shift to $\epsilon_{3s} - \epsilon_{np} + \Delta + i\Gamma_n/2$, where Γ_n is the width of the $3s3p^6np^1P$ state, and Δ is the usual resonance shift. Diagram (d) contributes to these resonances when $p = 3p$, $q = 3s$, $k' = np$, and $r = 3p$. Most important is the real contribution arising from $-i\pi\,\delta(D)$ of the bottom denominator (with $r = 3p$) and the imaginary part from $i\Gamma_n/2$ in the other denominator. At resonance this part of diagram (d) is identically opposite that from diagram (a), and this cancelation causes the absorption windows in $\sigma(\omega)$. We "calculated" resonances positions as $-[\epsilon_{3s}(\text{exp}) - \epsilon_{np}]$, where $-\epsilon_{3s}(\text{exp})$ is the experimental[21] $3s$ removal energy (29.24 eV), and ϵ_{np} is the single-particle HF energy for $3s3p^6np^1P$. There is of course an infinite number of resonances leading to the $3s$ ionization threshold at 29.24 eV, but it was not practical to show this in Fig. 2. Our results for resonance energies and widths are compared with experiment in Table I. The difference between the experimental and "calculated" energies includes Δ and the correlation energy of the np electron with the remaining system. These could be calculated, but our aim was to obtain $\sigma(\omega)$, and we used the experimental energies in calculating $\sigma(\omega)$.

Comparing MBPT with the RPAE, the RPAE has an advantage in that one is effectively summing certain classes of diagrams to all orders in perturbation theory. In perturbation theory, however, one can include any type of diagram. Also, MBPT may be readily applied to open-shell atoms.[18,19] This has not yet been shown feasible for the RPAE. In Ref. 10 only one bound excited state was included, and the continuum approximated by eleven terms. In the present work, for each l value, ten bound excited states were explicitly included, and the remainder included by our n^{-3} rule.[17] The continuum was described by thirty points for each l value. An advantage of MBPT is that the contributions from individual diagrams may be identified with distinct physical processes. One of our principal results is that when Hartree-Fock continuum states are used, the most important correction term is diagram 1(c) representing ground-state correlations.

In Ref. 10 correlations with $3s$ electrons were not included, thereby omitting the resonances. However, in a recent abstract[22] Amusia *et al.* report resonance profiles in good agreement with experiment[3] using the RPAE.

This calculation shows that good results for $\sigma(\omega)$ for Ar I (and presumably other rare gases) including resonances may be obtained in a low-order perturbation calculation in disagreement with Wendin's conclusions.[14] Wendin had to go to infinite order because he did not use the appropriate $(5p)^5\,^2Pkd^1P$ HF states. It is important in these calculations that the potential include the contributions from diagrams of Fig. 1(b) when p and q are in the same subshell. This corresponds to use of the HF potential for $(3p)^5kd^1P$ continuum states[10] and leads to a repulsive exchange term rather than an attractive exchange potential, and it changes the continuum wave functions qualitatively.

In conclusion, good results (except for resonances) are obtained with HF continuum states and only diagrams of Figs. 1(a) and 1(c), which includes ground-state correlations. Some improvement is obtained from the diagram of Fig. 1(f) between 30 and 45 eV.

We wish to emphasize that this calculation was in large part stimulated by the high-precision

data of Madden, Ederer, and Codling.[3]

We wish to acknowledge very helpful discussions with Dr. David L. Ederer, Dr. Robert P. Madden, Dr. Paul Fishbane, Dr. J. W. Cooper, and Dr. A. Weiss. We are also grateful to Dr. D. L. Ederer for communicating details of experimental results.

*Work supported in part by Aerospace Research Laboratories, Office of Aerospace Research, U. S. Air Force, Contract No. F33615-69-C-1048.

[1]G. V. Marr, *Photoionization Processes in Gases* (Academic, New York, 1967).

[2]J. A. R. Samson, Advan. At. Mol. Phys. 2, 177 (1966).

[3]R. P. Madden, D. L. Ederer, and K. Codling, Phys. Rev. 177, 136 (1969).

[4]A. P. Lukirskii, I. A. Brytov, and T. M. Zimkina, Opt. Spektrosk. 17, 438 (1964) [Opt. Spectrosc. 17, 234 (1964)].

[5]D. L. Ederer, Phys. Rev. Lett. 13, 760 (1964).

[6]J. W. Cooper, Phys. Rev. 128, 681 (1962).

[7]S. T. Manson and J. W. Cooper, Phys. Rev. 165, 126 (1968).

[8]M. Ya. Amusia, N. A. Cherepkov, L. V. Chernysheva, and S. I. Sheftel, Phys. Lett. 28A, 726 (1969).

[9]A. F. Starace, Phys. Rev. A 2, 118 (1970).

[10]M. Ya. Amus'ya, N. A. Cherepkov, and L. V. Chernysheva, Zh. Eksp. Teor. Fiz. 60, 160 (1971) [Sov. Phys. JETP 33, 90 (1971)].

[11]R. D. Chapman and R. J. W. Henry, Astrophys. J. 173, 243 (1972).

[12]D. J. Kennedy and S. T. Manson, Phys. Rev. 5, 227 (1972).

[13]H. A. Bethe and E. E. Salpeter, *Quantum Mechanics of One- and Two-Electron Atoms* (Academic, New York, 1957), p. 252.

[14]G. Wendin, J. Phys. B: Proc. Phys. Soc., London 5, 110 (1972).

[15]K. A. Brueckner, Phys. Rev. 97, 1353 (1955), and *The Many-Body Problem* (Wiley, New York, 1959).

[16]J. Goldstone, Proc. Roy. Soc., Ser A 239, 267 (1957).

[17]H. P. Kelly, Advan. Chem. Phys. 14, 129 (1969).

[18]H. P. Kelly and A. Ron, Phys. Rev. A 5, 168 (1972).

[19]R. L. Chase and H. P. Kelly, Phys. Rev. A 6, 2150 (1972).

[20]T. Ishihara and R. T. Poe, Phys. Rev. A 6, 111 (1972).

[21]K. Siegbahn *et al.*, Nova Acta Regiae Soc. Sci. Upsal. 20, 1 (1967).

[22]M. Ya. Amusia, V. K. Ivanov, N. A. Cherepkov, and L. V. Chernysheva, in *Seventh International Conference on the Physics of Electronic and Atomic Collisions, Abstracts of Papers, 1971,* edited by J. B. Hasted (North-Holland, Amsterdam, 1971).

Field Calibration Using the Energy Distribution of Field Ionization*

Toshio Sakurai and Erwin W. Müller
Department of Physics, The Pennsylvania State University, University Park, Pennsylvania 16802
(Received 4 January 1973)

The accuracy of data obtained by field-ion microscopy is often limited by a ±15% uncertainty of converting measured voltages into field strengths. Plotting the difference of relative energy deficits of free-space ionized H_2, D_2, or Kr for sets of two applied voltages against the logarithm of the voltage ratios yields a field factor k. The surface field $F_0 = V/kr_t$ is obtained with the 3% accuracy by which the tip radius r_t can be known. The method is applicable to all metals accessible to field-ion microscopy.

Field-ion microscopy[1] is increasingly used for quantitative investigations of surface phenomena such as field adsorption of noble gases,[2] or surface migration and surface binding energy[3-5] of individual atoms. All the data obtained require knowledge of the field strength F_0 at the tip surface, yet only the applied voltage V can be measured with any accuracy. A proportionality factor $\beta = F_0/V$ may be calculated for the quite unrealistic spherical case, or the better approximation of electrode geometry by confocal paraboloid, hyperboloid, or sphere-on-cone configurations. However, in real experiments the tip geometry is more complicated, with local radii varying over the emitting area and usually unknown shapes of the tip shank. Thus an experimental determination of β directly from emission data is most desirable. It may be surprising that essentially all field-ion data available are based on a calibration by Müller and Young,[6] who, assuming the validity of the Fowler-Nordheim equation, used field electron emission from a field-evaporated tip to determine the best image field (BIF) of tungsten in helium to be about 4.5 V/Å, with a small dependence on the tip radius. The accuracy of this calibration was estimated to be not better than ±15%, although for a given tip the best image voltage can be reproduced to within 1